Chinese Chemical Letters 35 (2024) 108587

Contents lists available at ScienceDirect

Chinese Chemical Letters

journal homepage: www.elsevier.com/locate/cclet

Plasmon-enhanced photocatalytic oxidative coupling of amines in the air using a delicate Ag nanowire@NH_2-UiO-66 core-shell nanostructures

Yuan Zhang[a,b,c,1], Shenghao Gong[a,b,c,1], A.R. Mahammed Shaheer[a,c], Rong Cao[a,b,c,*], Tianfu Liu[a,b,c,*]

[a] Fujian Science Technology Innovation Laboratory for Optoelectronic Information of China, Fuzhou 350108, China
[b] College of Chemistry and Materials Science, Fujian Normal University, Fuzhou 350007, China
[c] State Key Laboratory of Structural Chemistry, Fujian Institute of Research on the Structure of Matter, Chinese Academy of Sciences, Fuzhou 350002, China

ARTICLE INFO

Article history:
Received 12 April 2023
Revised 4 May 2023
Accepted 17 May 2023
Available online 20 May 2023

Keywords:
Metal-organic frameworks
Plasmonic silver nanowires
Photocatalyst
Core-shell nanostructure
Oxidative coupling of amines

ABSTRACT

MOF-based core-shell structures with high surface area, abundant active sites, and broad absorption bands are viable alternatives to traditional single-component photocatalysts. In this report, we describe the design and construction of delicate Ag nanowires@NH_2-UiO-66 with a core-shell structure for use as photocatalysts in imine synthesis under light. The optimized composites exhibited 80% imine production, which was higher than both MOF and Ag NWs. The significant improvement in photocatalytic activity under light may be attributed to the plasmonic effect of silver nanowires and their core-shell structure, which promotes the separation of electron-hole pairs. Moreover, the photocatalytic activity of the core-shell nanostructure may provide valuable insight into the design and construction of MOF-based composite photocatalysts for oxidative coupling of amines.

Imines are a class of active intermediates for dyes, biochemistry, and pharmaceuticals [1–3]. Synthesizing imines using environmentally friendly methods is becoming increasingly important to meet the demand that drives catalysis research. Since Ohtani *et al.* synthesized imines with palladium@TiO_2 photocatalyst [4], several decades ago, an increasing number of studies have focused on photocatalytic oxidative amine coupling [5–7]. It is generally believed that electrons in the conduction band (CB) of photocatalysts react with oxygen molecules and generate active oxygen species. These active oxygen species are the determining factors for the oxidate amines and facilitate the coupling of amines [6,8]. Recently, composites that could expand the optical absorption range, reduce the band gap and promote the separation of photoelectron-hole pairs have been chosen as excellent photocatalysts to achieve the oxidation of amines [9–11].

Porous photoactive materials such as metal-organic frameworks (MOFs), and covalent organic frameworks (COFs) with more active sites, and a broader absorption band are viewed as potential candidates to form composites [12,13]. So far, these composites used for oxidative coupling of amines are generally composed of MOFs and other materials, such as CdS and Ce, that have matching CB with MOFs, thereby constructing the rapid charge transport channels and reservoir for the electrons [14,6]. It is evident that these systems could only absorb a narrow spectrum of UV–visible light range. In order to maximize solar energy utilization, researchers have developed metal nanoparticles that uniquely absorb visible and near infrared wavelengths through confined coherent electron cloud oscillation in the conduction band referring to localized surface plasmon resonance (LSPR) [15,16]. In addition, some literature has reported loading metal nanoparticles on MOFs to synthesize amines [17]. However, very few research studies have constructed core-shell structures containing MOFs and metal nanoparticles, which differ from loading systems to promote the photocatalytic oxidative coupling of amines.

Herein, we fabricated NH_2-UiO-66 coating on Ag nanowires (NWs) with absorption at a more comprehensive UV-visible and infrared light range. Ag NWs are noted for their mechanical flexibility and high transmittance in the near infrared (NIR) [18]. NH_2-UiO-66 is a classical MOF that exhibits excellent chemical stability, high surface area and efficient light absorption ability [19–21]. More importantly, the zeta-potential of NH_2-UiO-66 is contrary to the Ag NWs in acidic pH range, which help to form the core-shell structure through electrostatic interaction [22,23]. The composite

* Corresponding authors.
E-mail addresses: rcao@fjirsm.ac.cn (R. Cao), tfliu@fjirsm.ac.cn (T. Liu).
[1] These authors contributed equally to this work.

https://doi.org/10.1016/j.cclet.2023.108587
1001-8417/

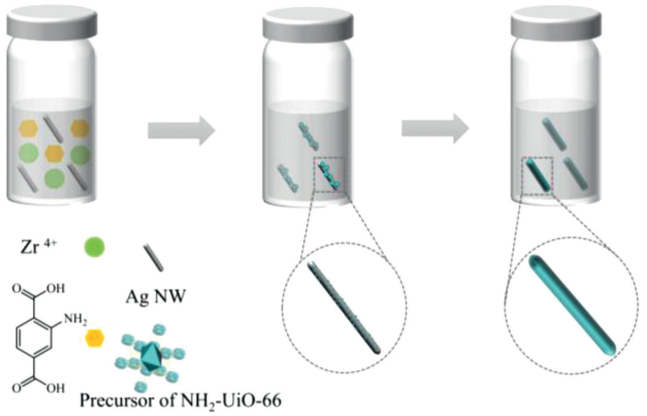

Scheme 1. Synthetic process of Ag NWs@ NH_2-UiO-66.

Ag NWs@NH_2-UiO-66 exhibited significantly enhanced photocatalytic activity of coupling imines under mild conditions in the air atmosphere. The research could offer valuable reference for the design and construction of MOF-based composite photocatalysts for oxidative coupling of amines.

In a typical experiment, a one-pot synthesis of $ZrCl_4$, NH_2-BDC, and DMF solution containing pre-synthesized Ag NWs yielded Ag NWs@NH_2-UiO-66 (A@U). Briefly, the positively charged precursors of NH_2-UiO-66 were anchored on the surface of negatively charged Ag NWs *via* electrostatic interaction. Then, the MOF crystal nucleus was anchored on the Ag NWs and increasingly grown on the Ag NWs to form a core-shell (Scheme 1). The thickness of the NH_2-UiO-66 sheath was controlled by the cyclic growth time of precursors on the Ag nanowires surface to achieve the optimal catalytic performance of the A@U core/sheath nanowires.

Two samples of Ag nanowires with 1 and 2 cycle coating layers, named A@U-1, and A@U-2, respectively, were synthesized to optimize catalytic performance. The PXRD patterns of A@U-1, A@U-2 and NH_2-UiO-66 were in good agreement with the simulation, which indicated the successful construction of the composite structure (Fig. 1a). It is worth noting that, after removing the Ag NWs characteristic diffraction peaks, the diffraction peaks in the range of 6°−9° are exactly in agreement with NH_2-UiO-66 (Fig. 1b). The N_2 adsorption-desorption isotherms of composites and NH_2-UiO-66 also exhibited typical type-I isotherms (Fig. S1 in Supporting information). To investigate the morphology and particle size of composites, A@U were characterized by scanning electron microscopy (SEM) and high-resolution TEM (HRTEM). As shown in Fig. 1c, the surface of Ag NWs was smooth and uniform thickness of NH_2-UiO-66 increased over cyclic time (Fig. 1d, Figs. S2 and S3 in Supporting information). The TEM images suggested that the thickness of the NH_2-UiO-66 coating layer of A@U-1 and A@U-2 was about 40 and 70 nm, respectively (Fig. 1e and Fig. S2). The corresponding high-resolution TEM (HRTEM) image (inset in Fig. 1e) showed the lattice fringes with an interplanar spacing of 1.21 nm, which matched with the (111) crystal plane of NH_2-UiO-66. Moreover, the energy-dispersive X-ray spectroscopy (EDS) elemental mapping (Fig. 1f) and DRIFTS (Fig. S4 in Supporting information) of A@U-1 supported the delicate structure that proportional NH_2-UiO-66 well-bound on the Ag nanowires.

The elemental valence states of composites were investigated by XPS. As shown in Fig. 2a, the survey spectrum suggests that A@U-1 contains C, O, N, Zr and Ag elements, which agrees with the EDS mapping. The high-resolution C 1s spectrum can be split into three peaks, at 284.8, 286.43 and 288.71 eV, which could be attributed to carbon-carbon single bond, carbon-oxgyen single bond, and carbon-oxgyen double bond group in the NH_2-UiO-66 (Fig. 2b). The O 1s spectrum shows the three peaks at 530.44, 531.84 and 533.35 eV, ascribed to absorbrd lattice oxygens, oxygens of COOH groups and oxygen vacancies, respectively (Fig. 2c). Two peaks centered at 399.28 eV (-NH_2), and 401.20 eV (-NH_3^+) can be seen in the N 1s spectrum (Fig. 2d). There are two peaks in the Zr spectrum that can be related to Zr $3d_{5/2}$ (182.68 eV), and Zr $3d_{3/2}$ (185.10 eV) (Fig. 2e) [6,24]. Evidently, the spectrum of the Ag 3d region can be fitted to two peaks for Ag $3d_{3/2}$ (374.22 eV) and Ag $3d_{5/2}$ (368.23 eV) of metallic Ag state (Fig. 2f).

UV-visible analysis was performed (Fig. 3a) to understand the optical absorption abilities of core-shell structures. Apparently, NH_2-UiO-66 could only absorb a narrow range of UV-visible light, while A@U-X exhibited wider absorption at the range of 400–800 nm, paving the way to utilize more optical energy. Meanwhile, the bandgaps of NH_2-UiO-66, and A@U-X (Fig. 3b) were calculated by tauc plot by using diffused reflectance spectra [17]. Specifically, the bandgap of NH_2-UiO-66, A@U-1, and A@U-2 is 2.83, 2.54 and 2.59 eV, respectively. It is worth noting that the A@U-1 which has a thinner coating layer exhibited a narrower bandgap than the thicker one, indicating the consequent catalytic performances of A@U-1. In order to reveal the core-shell structures abilities of separating photoelectron-hole pairs, composites were tested by

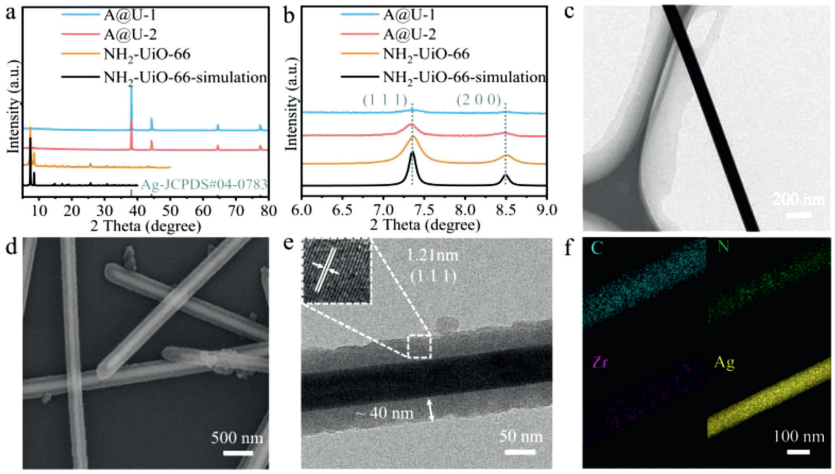

Fig. 1. (a) PXRD patterns of A@U-1, A@U-2 and NH_2-UiO-66. (b) PXRD patterns of A@U-1, A@U-2 and NH_2-UiO-66 in 6°−9°. (c) TEM images of Ag NWs. (d) SEM image and (e) TEM image of A@U-1 heterogeneous nanostructure. Inset in (e) local magnification of HRTEM images of A@U-1 heterogeneous nanostructure. (f) EDS-Mapping spectra of A@U-1.

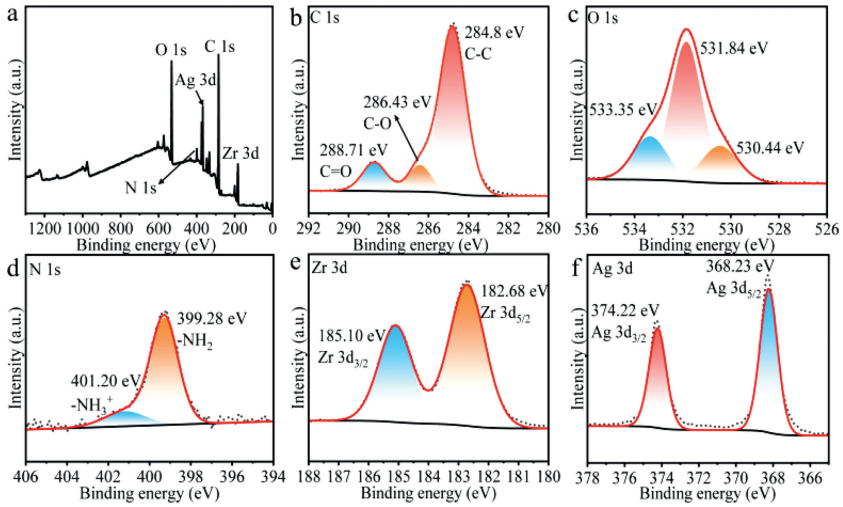

Fig. 2. (a) Survey spectrum and high-resolution (b) C 1s, (c) O 1s, (d) N 1s, (e) Zr 3d, and (f) Ag 3d spectra.

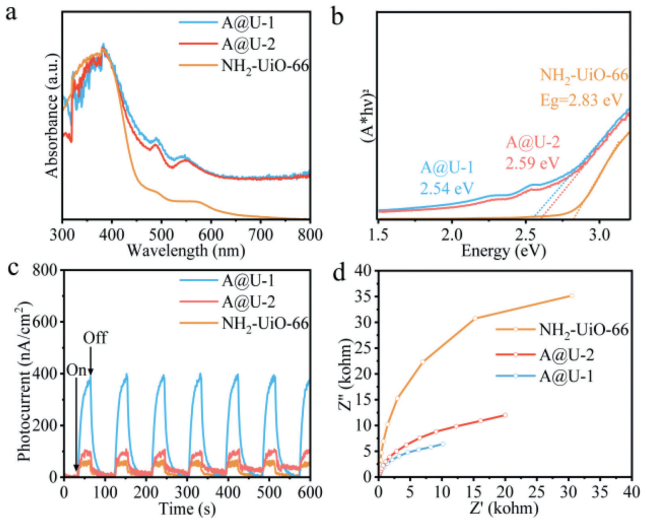

Fig. 3. (a) UV–vis DRS spectra of NH_2-UiO-66, A@U-1and A@U-2. (b) Tauc/Davis–Mott plots of NH_2-UiO-66, A@U-1 and A@U-2. (c) Transient photocurrent response of NH_2-UiO-66, A@U-1 and A@U-2. (d) Electrochemical impedance spectra curves of NH_2-UiO-66, A@U-1 and A@U-2.

Table 1
Photocatalytic oxidative coupling reaction of benzylamine.[a]

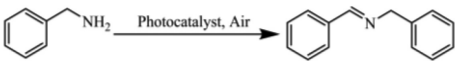

Entry	Catalyst	Quenching agent[b]	Air[c]	Light[d]	Yield (%)
1	NH_2-UiO-66	–	+	+	50
2	Ag NWs	–	+	+	14
3	A@U-1	–	+	+	80
4	A@U-2	–	+	+	62
5	A@U-1	–	–	–	–
6	–	–	+	+	6
7	A@U-1	–	N_2	+	7
8	A@U-1	BQ	+	+	14
9	A@U-1	KI	+	+	22
10	A@U-1	$K_2S_2O_8$	+	+	8

[a] Reaction conditions: amine (0.1 mmol), photocatalyst (15 mg), CH_3CN (3 mL), 300 W Xe lamp and 10 h.
[b] (+ or –) with or without a quenching agent.
[c] (+ or –) with or without air.
[d] (+ or –) with or without light. Yield was determined by ^1H NMR spectroscopic analysis.

photoelectrochemical measurements. As depicted in Fig. 3c, both A@U composites exhibited significantly enhanced photocurrent response abilities, which were higher than the NH_2-UiO-66. More importantly, the A@U-1 with thinner thickness exhibited the highest photocurrent response, indicating that the A@U-1 had the best ability to separate photoelectron-hole pairs. The electrochemical impedance spectroscopy (EIS) (Fig. 3d) also supported a similar conclusion, A@U-1 had the smallest radium, confirming its charge transfer resistance was lower than that of A@U-2.

To preliminarily evaluate the catalytic activity of A@U for the oxidative coupling of amines to imines, benzylamine was chosen as a substrate. When NH_2-UiO-66, Ag NWs, A@U-1 and A@U-2 were used as catalysts, the yields of imines were 50%, 14%, 80% and 62%, respectively (Table 1). As expected, due to its core-shell structure, A@U displayed better imine yields than the original single-component MOF. In addition, A@U-1 exhibited better catalytic activity under the light. Blank experiments in the absence of either light or catalyst showed only slight conversion of the substrates, confirming that the photocatalytic process drove the conversion of amines. The low benzylamine yield in N_2 indicated that oxygen was required to be involved in the photocatalytic oxidative coupling of amines. To demonstrate that the reaction was truly processed in a heterogeneous manner, the catalyst was filtered out during the reaction, and the results revealed that keeping the reaction under identical conditions for another 2 h did not lead to any conversion of benzylamine (Fig. S5 in Supporting information). In order to evaluate the cyclic stability of the catalyst for the benzylamine coupling reaction, A@U-1 was selected to investigate the stability of the catalyst after recovery (Fig. S6 in Supporting information). The PXRD patterns and FT-IR spectra of A@U-1 after three reaction cycles are well matched with those of the material before the reaction, which proves that A@U-1 has good photocatalytic benzylamine coupling cycle stability (Fig. S7 in Supporting information).

The semiconducting properties of NH_2-UiO-66 were measured using Mott-Schottky measurements (Fig. S8 in Supporting information) with three different frequencies. NH_2-UiO-66 displayed an n-type semiconductor, and its conduction band minimum (CBM) is −0.62 V *vs.* NHE, it is theoretically suitable for electrons transfered to O_2 to produce related reactive oxygen species (ROS, $E(O_2/{\cdot}O_2^-) = -0.33$ V *vs.* NHE) [25]. Considering the bandgap of NH_2-UiO-66 from tauc plot (2.83 V), the calculated valence band maximum (VBM) is +2.21 V *vs.* NHE. In comparison with the

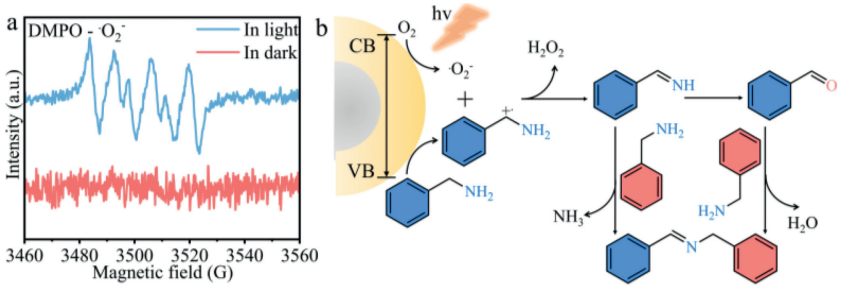

Fig. 4. (a) ESR spectra of A@U-1 containing DMPO. (b) Possible mechanism of the photocatalytic reaction.

previously reported systems (Table S1 in Supporting information), the delicate core-shell composite facilitates the coupling of amines under air, which is indicative that these core-shell systems possess a higher catalytic superiority over other silver nanocomposites. NH_2-UiO-66 shells in A@U can (1) stabilize and disperse silver nanowires; (2) increase the number of active sites; (3) accumulation of photoelectrons and transfer them to the active site. The outstanding catalytic ability could be summarized as follows: (1) Plasmon sensitization of plasmonic metal and semiconductor composite nanostructures has been considered as a functioning mechanism in photocatalysis [26]. When under resonant excitation of the LSPR of the Ag NWs, the electron from Ag NWs is transferred to NH_2-UiO-66 by plasmon quanta decay into an electron-hole pair [27]. As a result, wide-band gap NH_2-UiO-66 gain additional electrons and exhibit better photocatalytic activity. (2) The excellent photothermal behavior of composites could also convert optical radiation to thermal energy thus accelerating the catalytic reaction. (3) The porous characteristic of NH_2-UiO-66 makes sure it can efficiently absorb O_2 to promote the reaction. (4) The surface of the composite promotes the separation of electron-hole pairs. Under illumination, Ag NWs with LSPR effect will generate a significantly enhanced local electromagnetic field in the near-field region near the surface. The NH_2-UiO-66 located near the Ag NWs is affected by the strong electric field, and its intensity is several orders of magnitude larger than that of the far-field incident. Since the generation rate of electron/hole pairs is proportional to the locally excited light, the concentration of electron/hole pairs produced in this region of the NH_2-UiO-66 is greatly increased [28]. (5) The A@U-1 with thinner shell thickness shows better catalytic activity since the intensity of the near-field from LSPR decays with the distance from the surface of the Ag NWs, a thinner MOF layer will be under the influence of a stronger electric field on average, leading to superior catalytic activity. When the shell thickness becomes thicker, the Plasmon-Enhanced photocatalytic oxidative coupling of amines becomes weaker (Fig. S9 in Supporting information).

In order to explore the active species in the reaction, a series of quenchers were added to the reaction system (Table 1). These include *p*-benzoquinone (quenches superoxide radicals); potassium persulfate (quenches electrons) and potassium iodide (to quench holes). After adding three quenchants, the yield of imines decreased to a certain extent, indicating that superoxide radicals, photogenerated electrons and holes were involved in the reaction process. To identify the reactive oxygen species of the photocatalytic reaction, A@U-1 with better catalytic activity was detected with DMPO (Fig. 4a). In the dark background, there was no observable signal, while there was a typical sextet signal, which could be identified as a superoxide radical ($^{\cdot}O_2^-$), observed under the light. In addition, H_2O_2 and benzaldehyde were detected by NMR and GC–MS analysis (Fig. S10 in Supporting information). Above all, we propose a possible mechanism to synthesize amines with core-shell composites A@U-X (Fig. 4b). Step 1: Ag NWs is excited to yield plasmon quanta, which could be converted into electron-hole pairs of NH_2-UiO-66 *via* the composite's surface. Step 2: Electron-hole pairs are further separated on the surface, electrons activate O_2 to $^{\cdot}O_2^-$, meanwhile holes react with benzylamine generating carbocationic radicals. Step 3: A pair of $^{\cdot}O_2^-$ and carbocationic radicals react with each other and generate PHCH=NH intermediate and benzaldehyde. Step 4: PHCH=NH intermediate and benzaldehyde nucleophilic attacks another benzylamine forming the imine.

In conclusion, we constructed delicate Ag nanowires@NH_2-UiO-66 core-shell nanostructures as photocatalysts to oxidize amines and facilitate the coupling of amines. The A@U-1 composite further successfully synthesizes amines under air with a higher yield compared to both constituent parts. Moreover, the result reveals that in semiconductor-metal composite systems, the metal component with LSPR may take the lead during the photocatalytic oxidative coupling of amines. This work proposes a noble core-shell construction strategy that could offer valuable reference for the design and construction of MOF-based composite photocatalysts for oxidative coupling of amines.

Declaration of competing interest

The authors declare no competing financial interest.

Acknowledgments

The authors gratefully acknowledge the Fujian Science Technology Innovation Laboratory for Optoelectronic Information of China (Nos. 2021ZR105 and 2021ZZ103), financial support from the National Natural Science Foundation of China (Nos. 22071246 and 22033008).

References

[1] S. Kobayashi, Y. Mori, J.S. Fossey, M.M. Salter, Chem. Rev. 111 (2011) 2626–2704.
[2] S. Kobayashi, H. Ishitani, Chem. Rev. 99 (1999) 1069–1094.
[3] B.S.Holla M.Ashok, B. Poojary, Eur. J. Med. Chem. 46 (2007) 1095.
[4] B. Ohtani, H. Osaki, S.I. Nishimoto, T. Kagia, Chem. Lett. 21 (1985) 1075.
[5] F.Z. Su, S.C. Mathew, L. Mohlmann, et al., Angew. Chem. Int. Ed. 123 (2011) 683–686.
[6] H.L. Chen, C. Liu, W. Guo, et al., Catal. Sci. Technol. 12 (2022) 1812.
[7] W. Phasayavan, M. Japa, S. Pornsuwan, et al., J. Colloid Interf. Sci. 581 (2021) 719–728.
[8] K. Gao, H.J. Li, W J.H.W. Hou, ACS Appl. Mater. Interfaces. 13 (2021) 2779–2787.
[9] Y. Xiao, Y. Huang, S. Xue, J. Zhao, Appl. Catal. B 265 (2020) 118596.
[10] Z.Y. Zhai, X.N. Guo, G.Q. Jin, X.Y. Guo, Catal. Sci. Technol. 5 (2015) 4202–4207.
[11] Y. Xu, Y. Chen, W.F. Fu, Appl. Catal. B 236 (2018) 176–183.
[12] L. Jiao, Y. Wang, H.L. Jiang, Q. Xu, Adv. Mater. 30 (2018) 1703663.
[13] A. Dhakshinamoorthy, Z. Li, H. Garcia, Chem. Soc. Rev. 47 (2018) 8134–8172.
[14] Y. Song, R. Wang, X.Y. Li, et al., Chin. Chem. Lett. 33 (2021) 1283–1287.
[15] J. Perezjuste, I. Pastorizasantos, L. Lizmarzan, P. Mulvaney, Coord. Chem. Rev. 249 (2005) 1870–1901.
[16] Q.Q. Huang, Z.B. Fang, K. Pang, et al., Adv. Funct. Mater. 32 (2022) 2205147.
[17] C. Liu, Y.Y. Liu, Y.Z. Shi, J. Colloid Interf. Sci. 631 (2023) 154–163.
[18] D. Bellet, M. Lagrange, T. Sannicolo, et al., Materials 10 (2017) 570.
[19] Y. Bai, Y. Dou, L.H. Xie, et al., Chem. Soc. Rev. 45 (2016) 2327–2367.
[20] L. Shi, X. Zou, T. Wang, et al., Chin. Chem. Lett. 33 (2022) 442–446.

[21] T. Xia, Y.C. Lin, W.Z. Li, et al., Chin. Chem. Lett. 32 (2021) 2975–2984.
[22] S. Choi, J. Park, W. Hyun, et al., ACS Nano 9 (2015) 6626.
[23] A.H. Ibrahim, W.A. Eimehalmey, R.R. Haikal, et al., Inorg. Chem. 58 (2019) 15078–15087.
[24] X. Fang, S.B. Wu, Y.H. Wu, et al., Appl. Surf. Sci. 518 (2020) 146226.
[25] R. Chandra, M. Nath, Appl. Organoment. Chem. 34 (2020) e5951.
[26] C.X. Zhang, C.F. Xie, Y.Y. Gao, et al., Angew. Chem. Int. Ed. 61 (2022) e202204108.
[27] C. Sönnichsen, T. Franzl, T. Wilk, et al., Phys. Rev. Lett. 88 (2002) 077402.
[28] R.B. Jiang, B.X. Li, C.H. Fang, J.F. Wang, Adv. Mater. 26 (2014) 5274–5309.